Hole Doping in Epitaxial $MoSe_2$ Monolayer by Nitrogen Plasma Treatment

Yipu Xia[1†], Bo Wang[2,3†], Junqiu Zhang[1], Yue Feng[4], Bin Li[4], Xibiao Ren[3], Hao Tian[4], Jinpeng Xu[1], Wingkin Ho[1], Hu Xu[4], Chang Liu[4], Chuanhong Jin[2,3*], and Maohai Xie[1*]

† These authors contributed equally to this work

[1]Physics Department, The University of Hong Kong, Pokfulam Road, Hong Kong, China

[2]School of Physical Science and Technology, Lanzhou University, Lanzhou 730000, China

[3]State Key Laboratory of Silicon Materials, School of Materials and Engineering, Zhejiang University, Hangzhou, Zhejiang, 310027, China

[4]Department of Physics, Southern University of Science and Technology, Shenzhen, Guangdong 518055, China

[*]Corresponding authors, Emails: chhjin@zju.edu.cn (CHJ), mhxie@hku.hk (MHX)

ABSTRACT

Many transition-metal dichalcogenides, such as $MoSe_2$, are direct-gap semiconductors at monolayer thickness, which hold potentials in nano-electronics, optoelectronics, and some new concept spin- and valley-electronic applications. For device application, however, controllable doping of the materials is essential. Here we report hole doping of epitaxial $MoSe_2$ by nitrogen (N) plasma treatment with the aim of understanding the defect structure and its electronic characteristics. Examinations by annular dark field scanning transmission electron microscopy clearly reveal substitutional doping of N by replacing Se atoms in $MoSe_2$ monolayer upon N-plasma treatment, though creation of Se vacancies are also possible. Interestingly, we note an unexpectedly high concentration of 'dual defects', where both Se atoms in the top and bottom Se layers of $MoSe_2$ at the same lattice site are substituted by N and/or become vacant, suggesting a catalytic effect of defect formation. X-ray photoelectron spectroscopy and electron energy loss spectroscopy confirm the presence of N-Mo bonds. Photoemission spectroscopy reveals an impurity band as well as the Fermi level shift, confirming the p-type doping effect in $MoSe_2$ monolayer by N-plasma treatment. Consistent with the PES results, scanning tunneling spectroscopy measurement also reveal defect states peaked at 0.6~0.7 eV above the valance band maximum. The effectiveness of N-doping is discussed.

Keywords: Doping, TMD monolayer, MBE, STEM, spectroscopy

1. Introduction

Monolayers of transition metal dichalcogenides (TMDs), such as $MoSe_2$, are direct-gap semiconductors that have attracted extensive research attentions in recent years. They hold great promises for nano electronics, optoelectronics, and the new concept spin- and valley-electronic applications.[1-6] For device applications, it is essential for one to controllably dope the material so as to achieve and tune its p- and n-type conductivity. Various doping strategies have been experimented and applied to TMDs.[7-8] For example, both p- and n-type doping have been demonstrated through charge transfer via nitrogen dioxide and ion gel gate dielectrics.[9-10] Surface modification by, e.g., adsorbing potassium atoms, has also been shown successful to some extents to achieve electron doping.[11-12] Substitutional p-type doping in MoS_2 by using Nb has been reported,[13-15] while that of n-type doping by substituting Mo by Re has been reported recently as well.[16] Besides, post growth plasma treatment of the TMDs has been suggested as an alternative method to dope MoS_2 and WSe_2.[17-19]

Despite these efforts, it remains an issue to effectively dope TMDs for wide ranges of conductivity tunings. The very structures of the defects, their effects on crystal and electronic structures, etc., are not yet fully understood for many. In this work, *in situ* nitrogen (N) plasma treatment of epitaxial $MoSe_2$ monolayer grown by molecular-beam epitaxy (MBE) is investigated with an aim to understand the doping effect, the defect structure and electronic characteristics. By using annular dark field scanning transmission electron microscopy (ADF-STEM), electron energy loss spectroscopy (EELS) and X-ray photoelectron spectroscopy (XPS), angle resolved photoemission spectroscopy (ARPES), scanning tunneling microscopy and spectroscopy (STM/S), we establish that N doping is effected by substituting Se atoms in $MoSe_2$, giving rise to the hole doping effect. The former is evident from analyses of the STEM images as well as by observations of Mo-N bonds in the XPS, while the latter is shown by STS and (AR)PES the in-gap states closer to the valance band, as well as by the Fermi energy downward shift with increasing N dosage. We further observe an interesting catalytic 'dual defect' formation phenomenon, where both the top and bottom-layer Se in $MoSe_2$ at the same lattice site are substituted by N and/or become vacant. Finally, using reflection high-energy electron diffraction (RHEED), we observe continuous lattice constant change of $MoSe_2$ during N-plasma treatment, suggesting that compressive strains develop in $MoSe_2$ film upon N doping.

2. Results and Discussions

2.1. Substitutional doping of N in $MoSe_2$

Figure 1(a-c) shows the evolution of RHEED patterns of a sample surface during continuous N-plasma treatment of an as-grown $MoSe_2$ monolayer by MBE. As is seen, upon increasing N exposure time, the diffraction patterns become dimmer while the background becomes brighter, indicating an increasing roughness of the surface. Examinations of the samples by STM after the N-plasma treatment for different time periods (Figure 1(d-f)) reveal an increasing defect density with increasing nitridation time, consistent with the RHEED observations.

To examine the characteristics of the defects introduced by N doping, we carry out the ADF-STEM measurements of N-plasma treated samples. Figure 2(a) presents a STEM image of a sample that has undergone 30 min N-plasma treatment. Two magnified images as well as the corresponding line intensity profiles are shown on the right. It is seen that there are many dark-contrast holes in the images but with mainly two intensity variations. From the magnified images and line intensity profiles, we infer that these holes almost all occur at the Se sites of $MoSe_2$ lattice, so they appear to be Se vacancies from the first sight. To obtain a better understanding of the STEM contrast and establish the nature of these defects, we perform simulations using the QSTEM software of STEM contrasts for a $MoSe_2$ monolayer but containing different types of defects:[20] (i) two missing Se atoms at the same site, one from top and the other from the bottom Se layer in $MoSe_2$ (i.e., a dual vacancy defect), (ii) one of the Se vacancies in (i) is filled with a N atom while the other remains vacant (vacancy + impurity), and (iii) both Se vacancies in (i) are filled with N (an impurity pair), (iv) a single Se atom is missing in one of the Se layers (i.e., a single vacancy defect), and (v) one Se is substituted by a N atom (a single impurity). The simulated STEM images and the corresponding atomic model are shown in Figure 2(b-f), from which one notes that Se vacancy and substitutional N defect can hardly be distinguished by the STEM contrast. It is more difficult to identify N in experimental STEM considering the existence of HOPG substrate. On the other hand, there is an apparent difference between a single and the dual

(pair) defect. The reason is simple, by the STEM's Z-contrast mechanism, image contrast is proportional to $Z^{1.6\text{-}2.0}$ (where Z stands for atomic number). N (Z=7) substituting Se (Z=34) does not give rise much STEM contrast than a Se vacancy.[21] Therefore, based on the STEM results of Figure 2(a), we can only conclude that nitridation of $MoSe_2$ by plasma treatment has indeed resulted in defects at the Se sites, but whether these defects are Se vacancies or that substituted by N or both remain to be established by other characterizations (see below). Nevertheless, by a statistical analysis of the experimental STEM images, one notes that although single vacancy or impurity defects are dominant (having a density of $\rho_1 = \frac{No.\ of\ defects}{No.\ of\ lattice\ sites} \sim 13.6\%$), which expectedly reside in the top Se layer due to direct interaction with the plasma, there are also a substantial number of dual or pair defects (i.e., $\rho_2 \sim 4.37\%$ per lattice site, see Supporting Information).[22] This is somewhat unexpected. Indeed, if the dual (pair) defect formation is solely of a stochastic process, the density of the dual defect would approximately be $\rho_1^2 \approx 1.85\%$, which is much less than the value found by experiment. This suggests a catalytic effect where nucleation of the single defect may have promoted or induced a preferential Se vacancy formation and/or N-substitution in the other Se layer at the same lattice site of $MoSe_2$. The cause is yet unknown and it could be chemically more favorable or caused by a high local strain induced by a single defect formation in $MoSe_2$ monolayer.

To compare the stability and thus the likelihood of formation of various possible defect structures, we have performed density functional theory (DFT) calculations for the formation energies of the five defect configurations introduced above, i.e., a dual (Se) vacancy (VV), a vacancy + N impurity (VN), a dual N impurity (NN), a single Se vacancy (V), and a single N impurity (N). The formation energy is defined as $\Delta H_f = E_\alpha - E_0 + \sum_\alpha n_\alpha \mu_\alpha$, where E_α and E_0 are the total energy of the slab with and without defect α. μ_α is the chemical potential of atom α, and here is represented by the chemical potential in their bulk counterparts. n_α refers to the number of defect α. A negative value of n_α is adopted when foreign atom is added, while a positive value is adopted when the lattice atom is removed. For the two single defects, the calculated formation energies are ~2.626 eV and ~1.428 eV for vacancy (Figure 2e) and substitutional N (Figure 2f), respectively. So it would be more favorable to form a substitutional defect than a vacancy. Similarly, for dual defects, the formation energy of a dual vacancy (Figure 2b) is ~5.087 eV, much higher than that of a dual N (~3.507eV, Figure 2d) or the N + vacancy pair (~3.041 eV, Figure 2c). Base on the above, it seems that single defects preferably form, while dual defects, if form, will likely be the NV and NN rather than the vacancy pairs. In any case, substitutional N will dominate over vacancies, which will thus result in hole doping.

As noted earlier, while the experimental STEM data confirm the presence of point defects at the Se sites in $MoSe_2$ after the N-plasma treatment, they can hardly distinguish between a substitutional N and a Se vacancy defect. For the purpose of the latter, we further performed the EELS and XPS measurements and the results are shown in Figure 3. Firstly, in the EELS data, a broad peak centered at ~401 eV is evident (Fig. 3a), which signifies the presence of N in the sample. The XPS results of Fig. 3(b), on the other hand, reveal intensity peaks at 397.3 eV and 394.7 eV that are characteristic of the Mo-N and Mo-Se bonds, respectively.[23] Analysis of the Mo $3d_{5/2}$ peak at ~219 eV in the XPS also resolves a shoulder 0.3 eV above the main peak (Fig. 3c), again reflecting the presence of the Mo-N bonds.[17] Hence, we believe that the defects in $MoSe_2$ as introduced by N-plasma treatment and observed by STEM experiments contain at least, if not all, substitutional N. A dominant N impurity defects over vacancies in sample would give rise to a net hole doping, whereas Se vacancies would provide electrons instead.

2.2. P-type doping confirmed by UPS and STS measurements

Experimental assessment of the doping characteristics are made by using spectroscopic measurements such as (AR)PES and STS. These measurements have not only allowed us to observe the monotonic down-shifts of the Fermi level with increasing N dosage, confirming the hole doping effect and thus a dominant substitutional N defects in plasma-treated $MoSe_2$, but also revealed the defect states or impurity bands directly.

Fig. 4(a) presents a set of ARPES results obtained from an as-grown, 30-min and 60-min N plasma treated samples as marked. The valance bands are notably up-shifted relative to the Fermi energy (E_F = 0 eV) as the dosage of N increases. For example, the valance band maximum (VBM) at the Γ point is at 1.7 eV below E_F for the as-grown film, but shifted to -1.4 and -1.2 eV respectively after 30-min and 60-min plasma treatments. These correspond to the equivalent down-shifts of 0.3 eV and 0.5 eV of the Fermi level

relative to the band-edges, suggesting effective hole doping of the samples. Moreover, in the ARPES (e.g., the 60-min plasma treated sample in Fig. 4a), a dim band located at about -0.5 eV is also discernable, which is not present in the ARPES of pristine $MoSe_2$ monolayers. We believe this band is associated with N-doping, i.e., an impurity band. Similarly, STS data also reveal in-gap states close to the valence band edge (Fig. 4e).

Fig. 4(b) shows a set of integrated UPS spectra, again for an as-grown, 30-min and 60-min plasma treated samples as marked. Agreeing with the ARPES data, there are apparent upward shifts of the VBM relative to E_F (0 eV), evidencing an increasing hole concentration by increasing N dosage of the samples. So, N-plasma treatment must have resulted in a dominant substitutional doping of N at the Se sites instead of creating Se vacancies. Otherwise, if the sample treatment by plasma had resulted in more vacancies, an increasing electron concentration and thus up-shift of the Fermi level would be expected. The conclusion of substitutional N in favor of Se vacancy in $MoSe_2$ has been supported by the DFT calculation results as presented earlier.

Besides UPS/ARPES measurements, we have also taken some local spectroscopic measurements by the STS. Fig. 4(e) shows a spectrum taken at a defect as marked in Figs. 4(c) and 4(d). Clearly, there are in-gap states peaked at ~ 0.66 eV below the Fermi energy. Although the energy position of these states deviates slightly from that of the dim band in Fig. 4a (which is slightly above -0.5 eV), we believe they are of the same states, as the STS and ARPES measurements were performed on two different samples. Although the two samples were grown and treated under the same conditions, variation of the Fermi level is unavoidable between samples. When measured relative to the VBM at the Γ point, the defect states are seen to be at 0.6~0.7 eV above VBM in both ARPES and STS. These states are spatially localized. Away from the defects, STS measurement reveals no in-gap states but a spectrum similar to that of a pristine $MoSe_2$. Localization of the defect states have led to the nondispersive impurity band as revealed in the ARPES data (i.e., the flat dim band in Fig. 4a, right panel). Together with the large activation energy (i.e., 0.6~0.7 eV from the VBM), this seems to suggest that substitutional N does not behave as an ordinary shallow acceptor defect.

An important question then arises on the effectiveness of hole doping by the substitutional N. Indeed, there is an apparent inconsistency between the defect density and hole concentration as inferred from the Fermi energy shift. As mentioned, by analyses of the STEM data, we derive a concentration of point defects in the 30-min plasma treated sample to be ~ 11% (i.e., half of the 13.6% single defects per site plus 4.4% dual defects per site, where the factor 'half' is to account for 2 Se atoms per lattice site in $MoSe_2$), mostly substitutional N as discussed above. To affirm such a high concentration of N impurity, we also resort to XPS data, from which a concentration of ~10% of N may be estimated (i.e., by the ratio of peak intensities after due account is taken of the sensitivity factors, see Supporting Information). This is only slightly less than 11% derived from the STEM, implying that the majority of the defects are indeed substitutional N instead of Se vacancies.

If all these N impurities are electronically active and ionized, one expects a very high hole concentration in sample and thus a much larger Fermi energy shift than experimentally observed. Indeed, the 0.3-0.5 eV down-shifts of the Fermi level seen by experiments (Figs. 4a and 4b) only translate into minute hole concentrations by doping. The main reason lies, besides the compensating effect by electrons (e.g., by vacancies and charge transfer from the substrate), in the fact that the activation energy of N defects are large (0.6~0.7eV), so at room temperature and 77 K, at which our ARPES and STS experiments were performed, only a minute fraction of the dopants becomes ionized and contributes to holes. As one increases temperature, higher concentrations of holes and consequently a larger shift of the E_F may be expected. On the other hand, the relatively high activation energy of N dopants may reflect a much reduced dielectric constants in 2D materials, which pose a challenge to effectively dope the materials by impurity in general.

Finally to supplement these experimental studies of defect states in $MoSe_2$, DFT calculations of the electronic structures of three possible defects, i.e., single and dual N impurities, and the N impurity + Se vacancy defect, are performed (refer to Supporting Information). The calculation results indeed show the presence of in-gap states close to valance band of $MoSe_2$ for both the single and dual N impurity defects, but the impurity + vacancy defect gives rise to an in-gap state closer to the conduction band and thus likely behaves as donors.[24]

2.3. Compressive strain introduced by N-doping

We have further monitored lattice constant change of $MoSe_2$ by N-doping. Figure 5 plots the evolution of in-plane lattice constant of $MoSe_2$ during the N-plasma treatment as measured by RHEED. Separate LEED measurements establish that epitaxial $MoSe_2$ and graphene substrate take an aligned (parallel) crystallographic relation (refer to Supplementary Information), therefore the in-plane lattice constants a of $MoSe_2$ can be readily derived by measuring the spacing D between the $(0\bar{1})$ and (01) diffraction streaks in RHHED (inset of Figure 5) and by making reference to D_{sub} of the substrate: $\frac{a}{a_{sub}} = \frac{D_{sub}}{D}$.[25] As is clear from Fig. 5, with increasing N dosage, the in-plane lattice constant a of $MoSe_2$ decreases continuously and after 30-min plasma treatment, the lattice has shrunken in average to ~ 0.324 nm from the initial value of ~ 0.329 nm. So there is about 1.5% compressive strain in film. This can be understood by the stronger and therefore shorter Mo-N bonds than Mo-Se bonds. Such strains will expectedly give rise to modifications of the electronic band structures and variation of the bandgap.

3. Conclusions

To conclude, we have demonstrated N doping in epitaxial $MoSe_2$ monolayer by *in situ* N plasma treatment. Combining STEM, EELS and XPS, we establish that N atoms substitute Se and thus act as acceptors. We note an unexpectedly high concentration of dual defects, where Se atoms at the top and bottom layers of the same site are both substituted by N or become vacant. It suggests a catalytic effect of N doping such that when a Se atom has been replaced by N, the second Se at the same site but in the other layer becomes less stable and prone to be substituted by N as well. UPS, ARPES and STS measurements all show a tuning of the Fermi level by N-doping, confirming the hole-doping effect or the acceptor property. ARPES and STS evidence the presence of in-gap defect states (impurity band) close to the valence band. An overall compressive strain is also found in film by N-doping.

4. Experimental Section

Molecular beam epitaxy of $MoSe_2$ and nitrogen plasma treatment

Depositions of monolayer $MoSe_2$ on graphene or HOPG were carried out in an Omicron UHV system having the background pressure in the low 10^{-10} Torr range. The flux of Mo was generated from an e-beam evaporator and that of Se was provided from a conventional Knudsen cell. Before $MoSe_2$ deposition, freshly cleaved HOPG or epitaxial graphene substrate was carefully prepared and for the latter, it was done by heating a SiC wafer at ~1100℃ in a Si flux. The temperature of $MoSe_2$ deposition was 500℃ and the deposition rate was 0.5 MLs/hr. A post-growth annealing process at 650℃ for 1 hr under a Se flux was adopted to smoothen the surface and remove domain boundary defects before nitrogen plasma treatment. The whole process was monitored by the RHEED operated at 10 keV. Nitrogen plasma was generated from radio-frequency (13.56 MHz) Oxford Applied Research plasma unit (HD25) operated at the RF power of 100 W. Nitrogen flow rate was 0.052 sccm. Nitrogen doping level was controlled by varying the exposure time and temperature of the sample for nitrogen plasma treatment, and the typical substrate temperature was 200℃ while the exposure time were within the range of 10-60 mins.

Scanning transmission electron microscopy and electron energy loss spectroscopy

The N-plasma treated $MoSe_2$ monolayer on HOPG was prepared through the micromechanical exfoliation process, and then transferred onto a molybdenum TEM grid with lacey carbon film for STEM and EELS observations. The paraffin wax used in micromechanical exfoliation process were repeatedly washed by acetone, which can substantially decrease the possible contamination. Annular dark-field (ADF)-STEM was performed in a so-called probe-corrected STEM (FEI Titan Chemi STEM) operated at 200kV. The convergence angle was set to be 21.4 mrad, and minimal acceptance angle of the ADF detector was set to ~65 mrad.

EELS measurements were conducted with a post-column spectrometer (Gatan Quantum 963) whose attainable energy resolution was better than 1eV. EEL spectra were recorded in diffraction mode where a selected-area aperture was used to limit the illuminated sample area down to 2 μm.

Ultraviolet/X-ray photoelectron spectroscopy, angle resolved photoemission spectroscopy

In-situ UPS was carried out right after N-plasma treatment with a base pressure of $\sim 2\text{x}10^{-9}$ mbar, a Helium discharge lamp was employed as He I source.

XPS measurements were performed in a Sengyang SKL-12 electron spectrometer equipped with a VG CLAM 4 MCD electron energy analyzer. X-ray source is a twin-anode (Mg/Al) source from VG (Model XR3E2). The XPS spectra were recorded using an achromatic Mg Kα excitation (1253.6 eV) at 10 kV, with an emission current of 15 mA. The system base pressures was $\sim 2x10^{-9}$ mbar.

The ARPES measurements were performed using a laboratory-based ARPES system consisting of a SPECS PHOIBOS 150 electron analyzer and a UVLS-600 UV lamp in the low 10^{-9} mbar range.

Scanning tunneling microscopy/spectroscopy

STM/STS measurements were carried out at 77K in a Unisoku scanning tunneling microscope (USM1500). It operated at the constant current mode at the tunneling current of 100pA.

Supporting Information

Supporting Information is available from the Wiley Online Library or from the author.

Acknowledgment

The work is financially supported by a General Research Fund (No. 17327316) from the Research Grant Council, Hong Kong Special Administrative Region and a NSFC/RGC joint research grant (No. N_HKU732/17 and 51761165024). The authors in ZJU thank Dr. Fang Lin for providing the improved wiener filter for the STEM image processing, and the Center for Electron Microscopy of Zhejiang University for the access to the microscope facilities.

References:

1. Neto, A. C.; Guinea, F.; Peres, N. M.; Novoselov, K. S.; Geim, A. K., The electronic properties of graphene. *Reviews of modern physics* **2009,** *81* (1), 109.
2. Xu, X.; Yao, W.; Xiao, D.; Heinz, T. F., Spin and pseudospins in layered transition metal dichalcogenides. *Nature Physics* **2014,** *10* (5), 343.
3. Wang, Q. H.; Kalantar-Zadeh, K.; Kis, A.; Coleman, J. N.; Strano, M. S., Electronics and optoelectronics of two-dimensional transition metal dichalcogenides. *Nature nanotechnology* **2012,** *7* (11), 699.
4. Chhowalla, M.; Jena, D.; Zhang, H., Two-dimensional semiconductors for transistors. *Nature Reviews Materials* **2016,** *1* (11), 16052.
5. Liu, H.; Jiao, L.; Yang, F.; Cai, Y.; Wu, X.; Ho, W.; Gao, C.; Jia, J.; Wang, N.; Fan, H., Dense network of one-dimensional midgap metallic modes in monolayer MoSe 2 and their spatial undulations. *Physical review letters* **2014,** *113* (6), 066105.
6. Jiao, L.; Liu, H. J.; Chen, J.; Yi, Y.; Chen, W.; Cai, Y.; Wang, J.; Dai, X.; Wang, N.; Ho, W. K., Molecular-beam epitaxy of monolayer MoSe2: growth characteristics and domain boundary formation. *New Journal of Physics* **2015,** *17* (5), 053023.
7. Gong, Y.; Lin, J.; Wang, X.; Shi, G.; Lei, S.; Lin, Z.; Zou, X.; Ye, G.; Vajtai, R.; Yakobson, B. I., Vertical and in-plane heterostructures from WS 2/MoS 2 monolayers. *Nature materials* **2014,** *13* (12), 1135.
8. Hao, L.; Liu, Y.; Gao, W.; Han, Z.; Xue, Q.; Zeng, H.; Wu, Z.; Zhu, J.; Zhang, W., Electrical and photovoltaic characteristics of MoS2/Si pn junctions. *Journal of Applied Physics* **2015,** *117* (11), 114502.
9. Fang, H.; Chuang, S.; Chang, T. C.; Takei, K.; Takahashi, T.; Javey, A., High-performance single layered WSe2 p-FETs with chemically doped contacts. *Nano letters* **2012,** *12* (7), 3788-3792.
10. Pu, J.; Yomogida, Y.; Liu, K.-K.; Li, L.-J.; Iwasa, Y.; Takenobu, T., Highly flexible MoS2 thin-film transistors with ion gel dielectrics. *Nano letters* **2012,** *12* (8), 4013-4017.
11. Fang, H.; Tosun, M.; Seol, G.; Chang, T. C.; Takei, K.; Guo, J.; Javey, A., Degenerate n-doping of few-layer transition metal dichalcogenides by potassium. *Nano letters* **2013,** *13* (5), 1991-1995.
12. Zhang, Y.; Chang, T.-R.; Zhou, B.; Cui, Y.-T.; Yan, H.; Liu, Z.; Schmitt, F.; Lee, J.; Moore, R.; Chen, Y., Direct observation of the transition from indirect to direct bandgap in atomically thin epitaxial MoSe2. *Nature nanotechnology* **2014,** *9* (2), 111-115.
13. Suh, J.; Park, T.-E.; Lin, D.-Y.; Fu, D.; Park, J.; Jung, H. J.; Chen, Y.; Ko, C.; Jang, C.; Sun, Y., Doping against the native propensity of MoS2: degenerate hole doping by cation substitution. *Nano letters* **2014,** *14* (12), 6976-6982.
14. Laskar, M. R.; Nath, D. N.; Ma, L.; Lee, E. W.; Lee, C. H.; Kent, T.; Yang, Z.; Mishra, R.; Roldan, M. A.; Idrobo, J.-C., p-type doping of MoS2 thin films using Nb. *Applied Physics Letters* **2014,** *104* (9), 092104.
15. Das, S.; Demarteau, M.; Roelofs, A., Nb-doped single crystalline MoS2 field effect transistor. *Applied Physics Letters* **2015,** *106* (17), 173506.
16. Zhang, K.; Bersch, B. M.; Joshi, J.; Addou, R.; Cormier, C. R.; Zhang, C.; Xu, K.; Briggs, N. C.; Wang, K.; Subramanian, S., Tuning the Electronic and Photonic Properties of Monolayer MoS2 via In Situ Rhenium Substitutional Doping. *Advanced Functional Materials* **2018**.
17. Azcatl, A.; Qin, X.; Prakash, A.; Zhang, C.;

Cheng, L.; Wang, Q.; Lu, N.; Kim, M. J.; Kim, J.; Cho, K., Covalent nitrogen doping and compressive strain in MoS2 by remote N2 plasma exposure. *Nano letters* **2016,** *16* (9), 5437-5443.
18. Khosravi, A.; Addou, R.; Smyth, C. M.; Yue, R.; Cormier, C. R.; Kim, J.; Hinkle, C. L.; Wallace, R. M., Covalent nitrogen doping in molecular beam epitaxy-grown and bulk WSe2. *APL Materials* **2018,** *6* (2), 026603.
19. Nipane, A.; Karmakar, D.; Kaushik, N.; Karande, S.; Lodha, S., Few-layer MoS2 p-type devices enabled by selective doping using low energy phosphorus implantation. *ACS nano* **2016,** *10* (2), 2128-2137.
20. Koch, C., Determination of core structure periodicity and point defect density along dislocations; Arizona State University: Phoenix, AZ, 2002. **2002**.
21. Hong, J.; Wang, C.; Liu, H.; Ren, X.; Chen, J.; Wang, G.; Jia, J.; Xie, M.; Jin, C.; Ji, W., Inversion Domain Boundary Induced Stacking and Bandstructure Diversity in Bilayer MoSe2. *Nano letters* **2017,** *17* (11), 6653-6660.
22. Zhen, F., Quantitative Electron Diffraction in Two Dimensional Materials and Automatic Data Processing in Electron Microscope, Zhejiang University. **2017**.
23. Sanjinés, R.; Wiemer, C.; Almeida, J.; Levy, F., Valence band photoemission study of the Ti□ Mo□ N system. *Thin Solid Films* **1996,** *290*, 334-338.
24. Qiu, H.; Xu, T.; Wang, Z.; Ren, W.; Nan, H.; Ni, Z.; Chen, Q.; Yuan, S.; Miao, F.; Song, F., Hopping transport through defect-induced localized states in molybdenum disulphide. *Nature communications* **2013,** *4*, 2642.
25. Li, B.; Guo, X.; Ho, W.; Xie, M., Strain in epitaxial Bi2Se3 grown on GaN and graphene substrates: A reflection high-energy electron diffraction study. *Applied Physics Letters* **2015,** *107* (8), 081604.

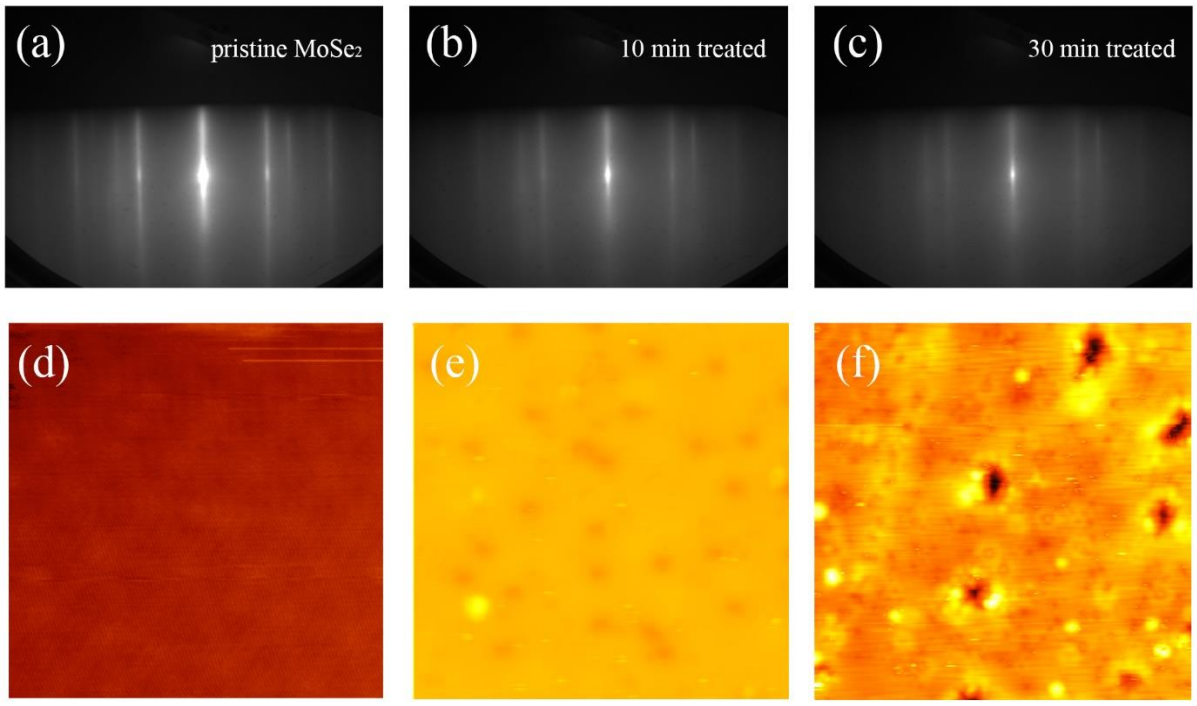

Figure 1. Effects of N-plasma treatment on the morphology of $MoSe_2$ surface. (a-c) RHEED patterns of an as-grown $MoSe_2$ (a) and under nitridation (200 °C, 0.052 sccm flow rate of N_2 and 100W RF power) for 10 min (b) and

30 min (c), respectively. (d-f) STM topographic images (size: 20 nm × 20 nm, sample bias: 2.0V) of an as-grown $MoSe_2$ (d), after 10 min (e) and 30 min (f) nitridation.

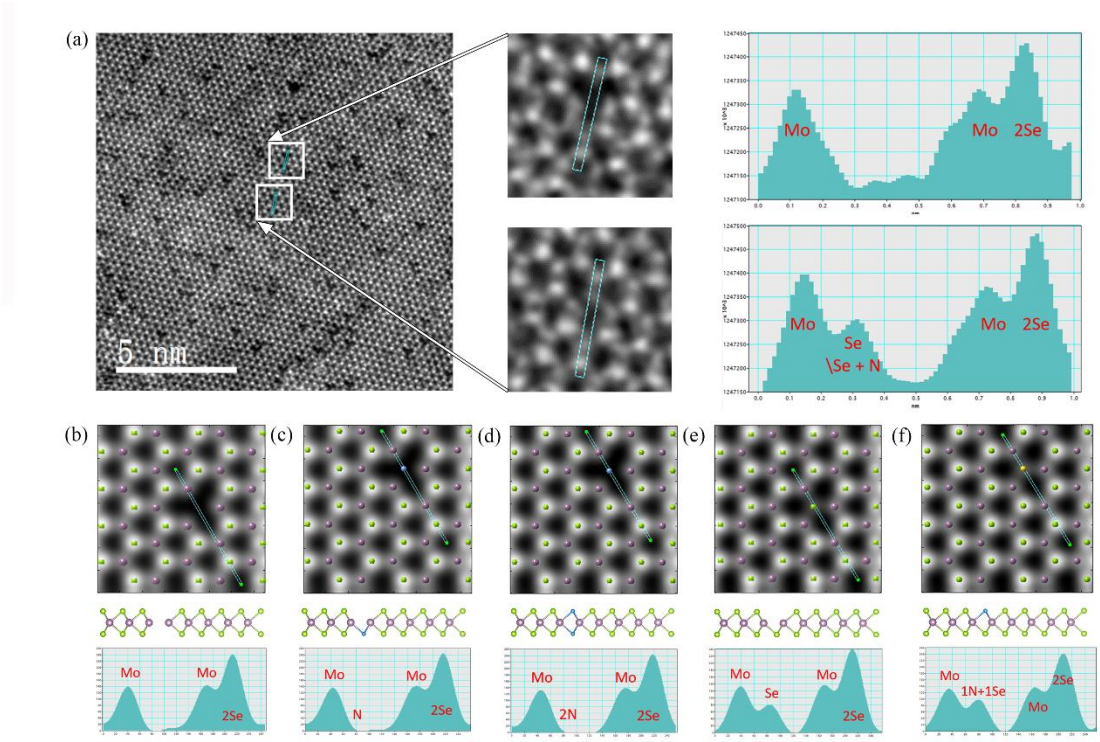

Figure 2. STEM analyses showing defects at Se sites after nitridation. (a) High-resolution ADF-STEM images (left panel) of a N-plasma treated $MoSe_2$ sample and the intensity line profiles (right) taken along the boxed regions drawn in the enlarged STEM micrographs (middle). (b-f) QSTEM simulated STEM images, their atomic structures and the derived intensity profiles of five possible defect configurations in $MoSe_2$ as depicted on the top, which contains Se vacancies, substitutional N on the Se sites, etc. (Mo, Se and N atoms are colored by purple, green and blue respectively, yellow represents Se in the top or bottom layer being substituted by a N atom).

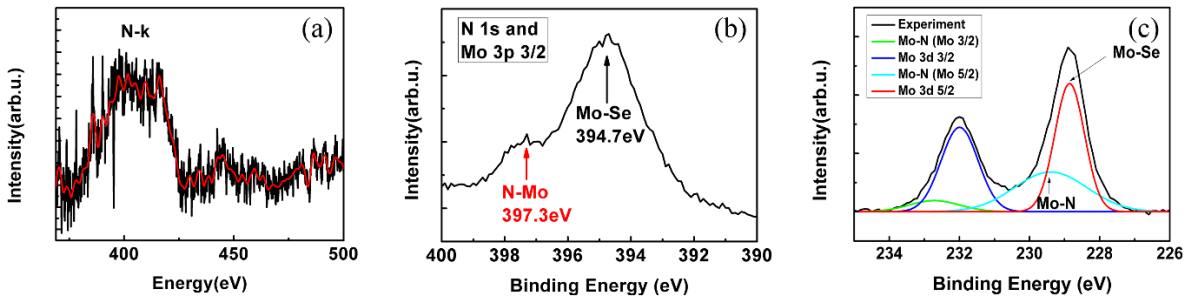

Figure 3. Spectroscopic analyses evidencing substitutional doping of N in sample. (a) Core-level EELS spectrum of a N-plasma treated sample, showing strong intensity peaks centered at 401 eV that evidences the presence of N atoms. (b,c) XPS spectra revealing N 1s (397.3 eV), Mo 3p (394.7 eV) and Mo 3d (229 eV) core levels in the Mo-N bonds. The color lines in (c) represent the curve-fitting results by multiple peaks Gaussian functions with linear baseline.

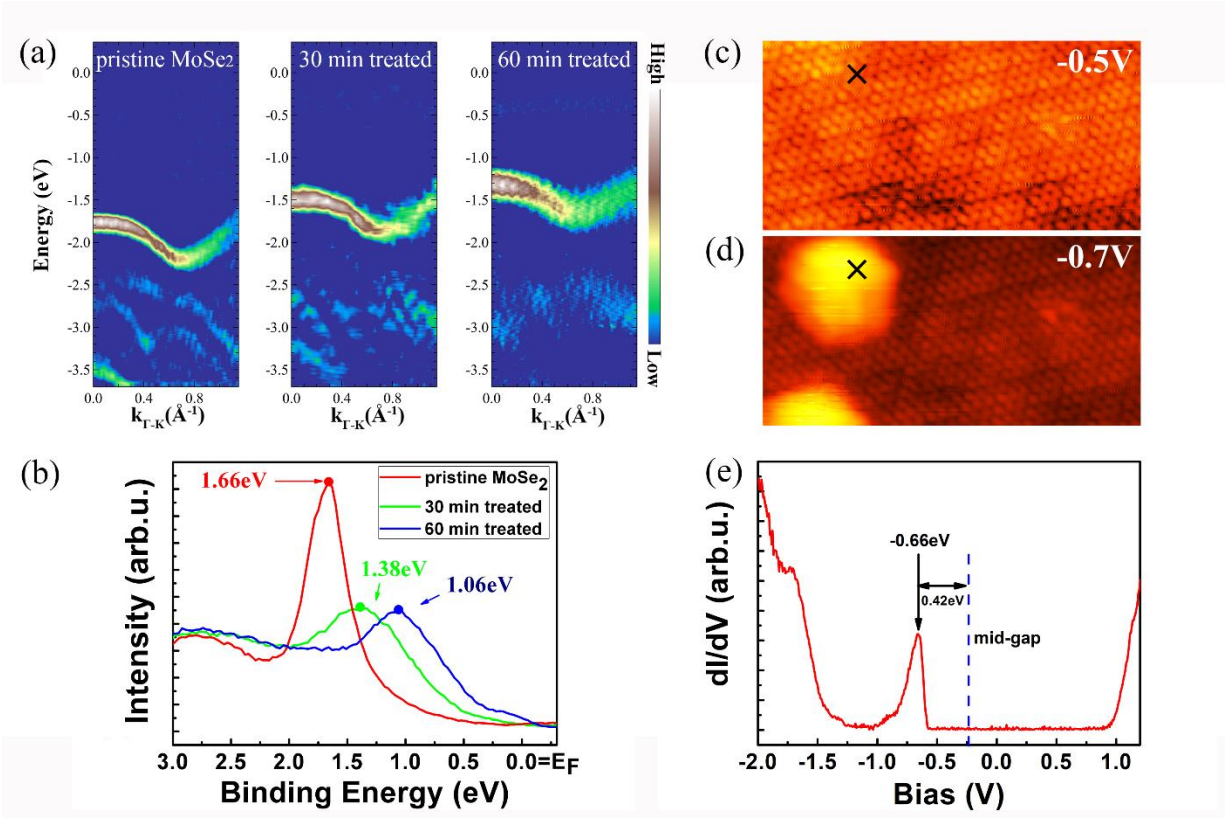

Figure 4. P-type doping in N-plasma treated $MoSe_2$ (a) ARPES spectra (second-derivative data) of $MoSe_2$ under different plasma treatment time, where the Fermi level shifts towards the valence band as the plasma treatment time

increases. The dim band at ~ -0.5 eV in the right panel (i.e., the 60-min treated sample) reflects the defect state. (b) integrated UPS spectra of pristine and doped $MoSe_2$, showing the Fermi level shifts after nitridation for 30 and 60 mins, respectively. (c,d) STM images (size: 10 nm × 5 nm) of the same region of a N-doped $MoSe_2$ sample but taken at different sample biases as indicated. (e) STS spectrum taken at the defect site as marked in (c) and (d). The tunneling current is 100pA. Impurity band appears closer to the valence band as marked by the black arrow.

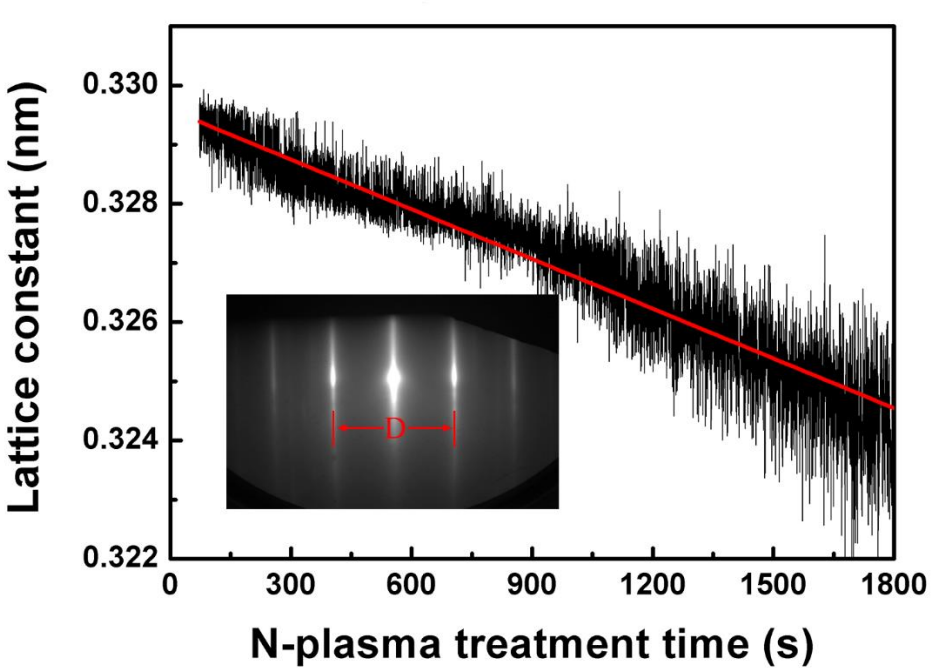

Figure 5. Doping induced compressive strain. Main figure: lattice constant variation as function of N-plasma exposure time. Inset: a RHEED pattern of $MoSe_2$, from which inter-diffraction streak spacing D is measured and used to derive a, the lattice constants shown.